REPORT DOCUMENTATION PAGE

Form Approved OMB No. 0704-0188

1. AGENCY USE ONLY (Leave blank)	2. REPORT DATE 23 June 1994	3. REPORT TYPE AND DATES COVERED Final Report

4. TITLE AND SUBTITLE

Semi-Empirical Potential Energy Surfaces of $(ArH_2O)^+$ System

5. FUNDING NUMBERS

F6170893W0493

6. AUTHOR(S)

Dr. Michael Baer, I.Last, H.Szichman

7. PERFORMING ORGANIZATION NAME(S) AND ADDRESS(ES)

Department of Physics and Applied Mathematics
Soreq Nuclear Research Center
Yavne 81800 Israel

8. PERFORMING ORGANIZATION REPORT NUMBER

SPC-93-4027

9. SPONSORING/MONITORING AGENCY NAME(S) AND ADDRESS(ES)

EOARD
PSC 802 BOX 14
FPO 09499-0200

10. SPONSORING/MONITORING AGENCY REPORT NUMBER

SPC-93-4027

11. SUPPLEMENTARY NOTES

12a. DISTRIBUTION/AVAILABILITY STATEMENT

Approved for public release; distribution is unlimited.

12b. DISTRIBUTION CODE

A

13. ABSTRACT (Maximum 200 words)

In order to study the exothermic charge transfer reaction $Ar^+ + H_2O \rightarrow Ar + (H2O)^+$ the semiempirical calculation of the $(ArH_2O)^+$ potential energy surfaces (PESs) is performed. These PESs are used to calculate the vibrational modes of the molecular species involved, in particular the highly excited vibronic bending modes of the reaction product $(H2O)^+$. It was found that the bending modes are affected by the stretching-bending coupling. It is shown that at superthermal collision energies the electrostatic approximation is not valid anymore as the electron hop occurs mainly in the strong interaction region. According to the results of the full scale calculation the reagents $Ar^+ + H_2O$ vibrational ground state is in near resonance with the excited bending $(0,9,0)$ state of the products $Ar + (H2O)^+$ along the whole interaction region. In a derivation based on simplifying assumptions (R.A. Dressler, J.A. Gardner, R.H.Salter, and E.Murad, *J.Chem.Phys.* 96, 1062 (1992)) the PESs were found to be significantly different in particularly the $Ar^+ + H_2O$ vibrational ground state crosses the $Ar + (H2O)^+$ bending manifold in the strong interaction region.

DTIC QUALITY INSPECTED 2

14. SUBJECT TERMS

15. NUMBER OF PAGES

40

16. PRICE CODE

17. SECURITY CLASSIFICATION OF REPORT UNCLASSIFIED	18. SECURITY CLASSIFICATION OF THIS PAGE UNCLASSIFIED	19. SECURITY CLASSIFICATION OF ABSTRACT UNCLASSIFIED	20. LIMITATION OF ABSTRACT UL

SEMIEMPIRICAL POTENTIAL ENERGY SURFACES OF $(ArH_2O)^+$ SYSTEM*

I.Last, H.Szichman and M.Baer

Department of Physics and Applied Mathematics
Soreq NRC, Yavne 81800, Israel

Abstract

In order to study the exothermic charge transfer reaction $Ar^+ + H_2O \rightarrow Ar + (H_2O)^+$ the semiempirical calculation of the $(ArH_2O)^+$ potential energy surfaces (PESs) is performed. These PESs are used to calculate the vibrational modes of the molecular species involved, in particular the highly excited vibronic bending modes of the reaction product $(H_2O)^+$. It was found that the bending modes are affected by the stretching–bending coupling. It is shown that at suprathermal collision energies the electrostatic approximation is not valid anymore as the electron hop occurs mainly in the strong interaction region. According to the results of the full scale calculation the reagents $Ar^+ + H_2O$ vibrational ground state is in near resonance with the excited bending (0,9,0) state of the products $Ar + (H_2O)^+$ along the whole interaction region. In a derivation based on simplifying assumptions (R.A.Dressler, J.A.Gardner, R.H.Salter, and E.Murad, *J.Chem.Phys.* 96, 1062 (1992)) the PESs were found to be significantly different in particularly the $Ar^+ + H_2O$ vibrational ground state crosses the $Ar + (H_2O)^+$ bending manifold in the strong interaction region.

1. Introduction

The purpose of this work is to calculate the $(ArH_2O)^+$ potential energy surfaces (PES) which describe the charge transfer process for the

$$Ar^+ + H_2O \rightarrow Ar + (H_2O)^+ \qquad (1)$$
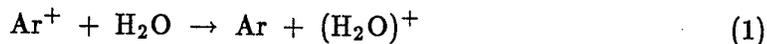
reaction.[1] The charge transfer process between rare gas atoms and molecules have received during the years considerable attention. However the theoretical studies in this field have mainly emphasized diatomic molecules and consequently systems such as $(ArH_2)^+$,[2-8] $(ArN_2)^+$,[9-10], $(ArCO)^+$,[9] $(HeH_2)^+$,[6] $(NeH_2)^+$,[6] and $(HeN_2)^+$ [6,11] were considered. No such studies are known to us for systems with triatomic molecules except for $(HeH_3)^+$ [12] and $(ArH_3)^+$ [13]. Our study is, probably, the first one dealing with the interaction of a rare gas ion with a triatomic molecule, such as H_2O.

The interaction between a rare gas ion (atom) and a polar molecule (molecular ion) is easily calculated in the asymptotic region where the interactions are determined by electrostatic forces such as charge-dipole forces in the case of the $Ar^+ + M$ system and polarization forces in the case of the $Ar + M^+$ system. However the polarization potential decreases very fast as R increases (namely like $1/R^4$) and so the charge-dipole interaction which decreases with R relatively slowly (as $1/R^2$) becomes the dominant interaction in this region. This fact was used by Dressler et al.[1] to construct their approximation for the $(ArH_2O)^+$ which assumes the charge-dipole interaction to be valid for the whole range. However this approximation is not valid at relatively small distances where interactions resulting from orbital overlap and charge delocalization become strong. The calculations of these interactions have to be performed either by an *ab initio* treatment or by semiempirical methods. In this work such a semiempirical treatment is presented.

The PES calculations of reactive systems are carried out mostly by employing diatomics-in-molecules (DIM) method.[14-18] The main advantage of this method is that it offers the possibility of expressing the energy of a polyatomic system in terms of diatomic potentials. The application of the DIM method to ionic systems such as $(ArH_2O)^+$ presents, however, some difficulties, mainly because of the charge delocalization and electrostatic interactions. These difficulties are successfully removed employing the diatomics-in-ionic-systems (DIIS) method which, like the DIM method, applies diatomic potentials to produce polyatomic PES.[19-20] However whereas within the DIM

1

one employs adiabatic potentials only, within the DIIS one incorporates both adiabatic as well as diabatic diatomic potentials. This modification enables the DIIS method to treat simple systems with charge delocalization, such as ionic rare gas clusters[8] or excited rare gas — halogen molecules $Xe_2^+Cl^-$.[19]

The charge transfer reaction is described as an nonadiabatic electronic transition and consequently at least two PESs are involved in the process. The charge transfer reaction (1) leads to the formation of the $(H_2O)^+$ molecular ion in the excited electronic state $\tilde{A}\ ^2A_1$. This is known to be a highly exothermic reaction and consequently the $(H_2O)^+$ ion is expected to be formed in highly excited vibronic bending states.[1] It follows that in order to understand the charge transfer process in the $(ArH_2O)^+$ system we need to calculate not only the $(ArH_2O)^+$ PESs but also the vibrational modes of the neutral and ionic species along the reaction coordinate.

2. Semiempirical treatment of the $(ArH_2O)^+$ PES

As was mentioned earlier the wave functions within the DIIS are expressed in terms of adiabatic and diabatic diatomic wave functions. The diabatic wave functions describe electronic configurations with localized charges, such as Ar^+H and ArH^+ but not $(ArH)^+$ which are presented in terms of the adiabatic functions.

In accordance with the DIIS method the polyatomic basis functions Φ are presented in terms of antisymmetrized products of atomic orbitals (AO) χ_i where i is the atom number. The $(ArH_2O)^+$ atoms are numbered as follows: the O-atom is $i = 1$, the H_a and H_b atoms are $i = 2$ and 3, and the Ar atom is $i = 4$. The s-AO is denoted by the atom number only whereas the p-AO is denoted by both the atom number and the orientation index. For example, the 1s AO of the H_a atom is χ_2, but the 2p AOs of the O atom are $\chi_{1x}, \chi_{1y}, \chi_{1z}$. We also distinguish between the two spin states χ (for $s = \frac{1}{2}$) and $\overline{\chi}$ (for $s = -\frac{1}{2}$)

As it is usually accepted in semiempirical methods, the O atom is described by the outer 2p-AOs ignoring the inner 1s and 2s electrons. In analogy with O the Ar atom is described in terms of the outer 3p-AOs. In addition we do an important simplification in which the P-symmetry of the Ar^+ is ignored and active valence AO $3p_z$, for example, is replaced by an s-AO. Consequently the Ar^+ and Ar are presented as χ_4 and $\chi_4\overline{\chi}_4$, respectively.

While describing the polyatomic basis functions we omit the symbol of antisymmetrization operator. The basis functions are built in such a way that in the asymptotic case of only two interacting atoms the interaction potentials coincide with the corresponding diatomic potentials. The $(ArH_2O)^+$ total spin is $S = \frac{1}{2}$ and its projection is assumed to be $S_z = +\frac{1}{2}$. The coordinate system we are using is as follows (Fig.1): the coordinate center is located at the atom O, the z-axis is directed toward the H_a atom, and the x-axis lies in the HOH plane. The location of the Ar atom is arbitrary.

Before treating the $(ArH_2O)^+$ system as a whole we consider the two molecular fragments of this system, namely H_2O and $(H_2O)^+$. The water molecule was treated already by the DIM method[14,21-22] but we can not use this representation as in our treatment H_2O (like $(H_2O)^+$) is not an isolated molecule but a fragment of a more complicated system. This imposes restrictions on the wave function presentation and the calculation procedure. Treating semiempirically H_2O and $(H_2O)^+$ we did the following: (a) a single set of basis functions and diatomic potentials were used to describe simultaneously both molecular fragments, (b) the calculated parameters of the ground $(\tilde{X}\ ^1A_1)$ H_2O and the ground $(\tilde{X}\ ^2B_1)$ and excited $(\tilde{A}\ ^2A_1)$ states of $(H_2O)^+$ fit as much as possible the corresponding empirical values, including the energy gaps of these states, (c) the H_2O and $(H_2O)^+$ basis functions are chosen in such a way that they can also describe the interactions with Ar and Ar^+, (d) the number of basis functions is kept as small as possible.

2.1 Ground state H_2O

In the usual language of molecular orbital theory the H_2O ground state configuration is:

$$\tilde{X}\ ^1A_1 \quad (1a)^2(2a)^2(1b_{xz})^2(3a)^2(1b_y)^2 \tag{2}$$

where a and b are symmetrical and anti-symmetrical orbitals, respectively. We describe the electronic structure of the $\tilde{X}\ ^1A_1$ state by the following basis functions:

$$\Phi_1 = \chi_{1x}\chi_{1y}\overline{\chi}_{1y}\chi_{1z}\overline{\chi}_2\overline{\chi}_3, \tag{3}$$

$$\Phi_2 = \chi_{1x}\chi_{1y}\overline{\chi}_{1y}\chi_{1z}\overline{\chi}_{1z}\overline{\chi}_2, \tag{4}$$

$$\Phi_3 = \chi_{1x}\overline{\chi}_{1x}\chi_{1y}\overline{\chi}_{1y}\chi_{1z}\overline{\chi}_2, \tag{4'}$$

$$\Phi_4 = \chi_{1x}\chi_{1y}\overline{\chi}_{1y}\chi_{1z}\overline{\chi}_{1z}\overline{\chi}_3, \tag{5}$$

3

$$\Phi_5 = \chi_{1x}\overline{\chi}_{1x}\chi_{1y}\overline{\chi}_{1y}\chi_{1z}\overline{\chi}_3, \tag{5'}$$

The first function correlates with the asymptotic $O(^3P)H_aH_b$ configuration. The functions Φ_i, $i = 2 - 5$ describe the configurations with the electron transfer from one of the H atoms to the O atom and correlate with the asymptotic $O^-(^2P)H_aH_b^+$ (Φ_2, Φ_3) or $O^-(^2P)H_a^+H_b$ (Φ_4, Φ_5). In our representation the $H_aH_b^+$ and $H_a^+H_b$ interactions are described as diabatic potentials, in contrast to the usual DIM approach where the adiabatic H_2^+ potentials are used. Also some of the O-H potentials will be assumed to be diabatic ones.

The diagonal matrix elements of the basis functions (3)-(5) are as follows:

$$H_{1,1} = U_{OH_a}(^2\Pi) + U_{OH_b}(^2\Pi) + W_{H_aH_b}(^3\Sigma), \tag{6}$$

$$H_{2,2} = W_{O-H_a}(^1\Pi) + \sin^2\theta\, U_{O-H_b^+}(^2\Sigma) + \cos^2\theta\, U_{O-H_b^+}(^2\Pi) + U_0, \tag{7}$$

$$H_{3,3} = W_{O-H_a}(^1\Sigma) + \cos^2\theta\, U_{O-H_b^+}(^2\Sigma) + \sin^2\theta\, U_{O-H_b^+}(^2\Pi) + U_0, \tag{7'}$$

$$H_{4,4} = U_{O-H_a^+}(^2\Pi) + \sin^2\theta\, W_{O-H_b}(^1\Sigma) + \cos^2\theta\, W_{O-H_b}(^1\Pi) + U_0, \tag{8}$$

$$H_{5,5} = U_{O-H_a^+}(^2\Sigma) + \cos^2\theta\, W_{O-H_b}(^1\Sigma) + \sin^2\theta\, W_{O-H_b}(^1\Pi) + U_0. \tag{8'}$$

$$U_0 = U_{H^+H}(^2\Sigma) - I_H + A_O, \tag{9}$$

where θ is the HOH angle, the W's and the U's are the adiabatic and the diabatic (with fixed charge location) potentials respectively (the diatomic states are shown in parentheses), I_H is the ionization potential of H and A_O is the electronic affinity of O.

The diabatic potentials U are derived from the appropriate adiabatic potentials in the way suggested within the DIIS method.[19-20] Let us consider first the homonuclear fragment H_2^+. In the framework of the ordinary approach the adiabatic states of this ion are Σ_g (attractive) and Σ_u (repulsive) which are the solutions of the equation

$$\begin{vmatrix} U - E & V \\ V & U - E \end{vmatrix} = 0 \tag{10}$$

Here U is the diabatic H^+H potential (the state symbol Σ is omitted) and V is the diabatic coupling term. Solving the inverse problem, i.e expressing U and V in terms of the two eigenvalues $E = W_g, W_u$, one obtains

$$U = \frac{1}{2}(W_g + W_u), \tag{11}$$

4

$$V = \frac{1}{2}(W_g - W_u),\tag{11'}$$

In the case of the heteronuclear fragment OH there are two (different) diabatic potentials, namely U_{OH} and $U_{O^-H^+}$, which fulfill the equation

$$\begin{vmatrix} U_{OH} - E & V_{OH} \\ V_{OH} & U_{O^-H^+} - E \end{vmatrix} = 0 \tag{12}$$

The corresponding eigenvalues are the adiabatic potentials of the ground state $W_{OH}(X^2\Pi)$ which correlates asymptotically with $O(^3P)H(^1S)$ and the excited state $W_{OH}(2\,^2\Pi)$ which correlates asymptotically with $O^-(^2P)H^+$. The exchange term V_{OH} is assumed to be a fitting function which will be determined later. Solving Eq.(12) yields for the diabatic potentials U_{OH} and $U_{O^-H^+}$ the expressions:

$$U_{OH} = \frac{1}{2}[W_{OH}(X^2\Pi) + W_{OH}(2^2\Pi) - W_d],\tag{13}$$

$$U_{O^-H^+} = \frac{1}{2}[W_{OH}(X^2\Pi) + W_{OH}(2^2\Pi) + W_d],\tag{13'}$$

where

$$W_d = \sqrt{[W_{OH}(2^2\Pi) - W_{OH}(X^2\Pi)]^2 - 4V_{OH}^2}\tag{14}$$

The exchange term V_{OH} has to be small enough to provide a real value for W_d.

Using the basis functions (3)-(5) one obtains the following non-zero off-diagonal matrix elements:

$$H_{1,2} = \cos^2\theta\, V_{OH_b},\tag{15}$$

$$H_{1,3} = \sin^2\theta\, V_{OH_b},\tag{15'}$$

$$H_{1,4} = V_{OH_a},\tag{15''}$$

$$H_{2,3} = \sin\theta\,\cos\theta\,[U_{O^-H_b^+}(^2\Sigma) + U_{O^-H_b^+}(^2\Pi)]\tag{16}$$

$$H_{4,5} = \sin\theta\,\cos\theta\,[W_{O^-H_b}(^1\Sigma) + W_{O^-H_b}(^1\Pi)]\tag{16'}$$

$$H_{2,4} = H_{3,5} = V_{H_2^+}\tag{17}$$

where V_{OH} and $V_{H_2^+}$ are the exchange terms of Eqs.(12) and (10), respectively.

5

2.2 Ground state $(H_2O)^+$

The $(H_2O)^+$ ground state configuration is (for notations see Eq.(2)):

$$\tilde{X}\,^2B_1 \quad (1a)^2(2a)^2(1b_{xz})^2(3a)^2(1b_y)^1 \qquad , \qquad (18)$$

We describe the electronic structure of the $\tilde{X}\,^2B_1$ state by following basis functions:

$$\Phi_1 = \chi_{1x}\chi_{1y}\chi_{1z}\overline{\chi}_{1z}\overline{\chi}_2, \qquad (19)$$

$$\Phi_2 = \chi_{1x}\overline{\chi}_{1x}\chi_{1y}\chi_{1z}\overline{\chi}_2, \qquad (19')$$

$$\Phi_3 = \chi_{1x}\chi_{1y}\chi_{1z}\overline{\chi}_{1z}\overline{\chi}_3, \qquad (20)$$

$$\Phi_4 = \chi_{1x}\overline{\chi}_{1x}\chi_{1y}\chi_{1z}\overline{\chi}_3, \qquad (20')$$

$$\Phi_5 = \chi_{1x}\overline{\chi}_{1x}\chi_{1y}\chi_{1z}\overline{\chi}_{1z}. \qquad (21)$$

The pairs of functions $(\Phi_1,\ \Phi_2)$ and $(\Phi_3,\ \Phi_4)$ correlate with the asymptotic $O(^3P)H_aH_b^+$ and $O(^3P)H_a^+H_b$ configurations, respectively, and the function Φ_5 correlates with the asymptotic $O^-(^2P)H_a^+H_b^+$ configuration. The diagonal matrix elements for the basis functions (19)-(21) are as follows:

$$H_{1,1} = W_{OH_a}(^2\Sigma^-) + \cos^2\theta\, W_{OH_b^+}(^3\Sigma^-) + \sin^2\theta\, W_{OH_b^+}(^3\Pi) + W_1, \qquad (22)$$

$$H_{2,2} = W_{OH_a}(^2\Pi) + \sin^2\theta\, W_{OH_b^+}(^3\Sigma^-) + \cos^2\theta\, W_{OH_b^+}(^3\Pi) + W_1, \qquad (22')$$

$$H_{3,3} = W_{OH_a^+}(^3\Sigma^-) + \cos^2\theta\, W_{OH_b}(^2\Sigma^-) + \sin^2\theta\, W_{OH_b}(^2\Pi) + W_1, \qquad (23)$$

$$H_{4,4} = W_{OH_a^+}(^3\Pi) + \sin^2\theta\, W_{OH_b}(^2\Sigma^-) + \cos^2\theta\, W_{OH_b}(^2\Pi) + W_1, \qquad (23')$$

$$H_{5,5} = U_{O^- - H_a^+}(^2\Pi) + U_{O^- - H_b^+}(^2\Pi) + W_2, \qquad (24)$$

where

$$W_1 = W_{H_2^+}(^2\Sigma_u) - I_H. \qquad (25)$$

and

$$W_2 = W_{H^+H^+} - 2I_H + A_O, \qquad (25')$$

Using the basis functions (19)-(21) one obtains the following non-zero off-diagonal matrix elements:

$$H_{1,2} = \sin\theta\,\cos\theta\,[W_{OH_b^+}(^3\Sigma^-) - W_{OH_b^+}(^3\Pi)], \qquad (26)$$

$$H_{3,4} = \sin\theta\,\cos\theta\,[W_{OH_b}(^2\Sigma^-) - W_{OH_b}(^2\Pi)], \qquad (26')$$

$$H_{3,5} = \sin\theta\, V_{OH_b}, \tag{27}$$

$$H_{4,5} = -\cos\theta\, V_{OH_b}, \tag{27'}$$

$$H_{2,5} = V_{OH_a}. \tag{27''}$$

2.3 Excited state $(H_2O)^+$

The $(H_2O)^+$ first excited state configuration is

$$\tilde{A}\ {}^2A_1 \quad (1a)^2(2a)^2(1b_{xz})^2(3a)^1(1b_y)^2 \tag{28}$$

We describe the electronic structure of the $\tilde{A}\ {}^2A_1$ state by following basis functions:

$$\Phi_1 = \chi_{1x}\chi_{1y}\overline{\chi}_{1y}\chi_{1z}\overline{\chi}_2, \tag{29}$$

$$\Phi_2 = \chi_{1x}\chi_{1y}\overline{\chi}_{1y}\chi_{1z}\overline{\chi}_3, \tag{29'}$$

$$\Phi_3 = \chi_{1x}\chi_{1y}\overline{\chi}_{1y}\chi_{1z}\overline{\chi}_{1z}, \tag{30}$$

$$\Phi_4 = \chi_{1x}\overline{\chi}_{1x}\chi_{1y}\overline{\chi}_{1y}\chi_{1z}. \tag{30'}$$

The functions Φ_1 and Φ_2 correlate with the asymptotic $O(^3P)H_aH_b^+$ and $O(^3P)H_a^+H_b$ configurations, respectively, and the functions Φ_3 and Φ_4 correlate with the asymptotic $O^-(^2P)H_a^+H_b^+$. The diagonal matrix elements of the basis functions (29)-(30) are as follows:

$$H_{1,1} = U_{OH_a}(^2\Pi) + W_{OH_b^+}(^3\Pi) + U_{H^+H}(^2\Sigma) - I_H, \tag{31}$$

$$H_{2,2} = W_{OH_a^+}(^3\Pi) + U_{OH_b}(^2\Pi) + U_{H^+H}(^2\Sigma) - I_H, \tag{31'}$$

$$H_{3,3} = U_{O^-H_a^+}(^2\Pi) + \sin^2\theta\, W_{O^-H_b^+}(^2\Sigma) + \cos^2\theta\, W_{O^-H_b^+}(^2\Pi) + W_2, \tag{32}$$

$$H_{4,4} = W_{O^-H_a^+}(^2\Sigma) + \cos^2\theta\, W_{O^-H_b^+}(^2\Sigma) + \sin^2\theta\, U_{O^-H_b^+}(^2\Pi) + W_2. \tag{32'}$$

Using the basis functions (29)-(30) one obtains the following non-zero off-diagonal matrix elements:

$$H_{1,3} = V_{OH_a}, \tag{33}$$

$$H_{2,3} = -\cos\theta\, V_{OH_b}, \tag{33'}$$

$$H_{2,4} = \sin\theta\, V_{OH_b}, \tag{33''}$$

$$H_{3,4} = \sin\theta\,\cos\theta\,[W_{O^-H_b^+}(^2\Sigma) - U_{O^-H_b^+}(^2\Pi)] \tag{34}$$

7

In the absence of the Ar atom the $\tilde{X}$ and $\tilde{A}$ states of $(H_2O)^+$ ionic molecule are uncoupled with one another.

2.4 $(ArH_2O)^+$ system

As it has been assumed by us, the electronic structure of Ar and Ar^+ is described in terms of s-symmetry χ_4 AO. Within the spirit of the DIIS method we will distinguish between configurations with the charge located on the H_2O molecule and with those where it is located on the Ar atom. We consider first the $Ar(H_2O)^+$ configuration states which correlate asymptotically with the configurations $ArOH_aH_b^+$, $ArOH_a^+H_b$, and $ArO^-H_a^+H_b^+$. The basis functions (19)-(21) and (29)-(30) present all possible orientations of the $(H_2O)^+$ electronic configuration. Adding the AOs of the Ar atom we obtain nine basis functions of the $Ar(H_2O)^+$ configuration. In what follows these basis functions along with the asymptotic atomic configurations are presented:

$ArOH_aH_b^+$:

$$\Phi_1 = \chi_{1x}\chi_{1y}\overline{\chi}_{1y}\chi_{1z}\overline{\chi}_2\chi_4\overline{\chi}_4, \tag{35}$$

$$\Phi_2 = \chi_{1x}\overline{\chi}_{1x}\chi_{1y}\chi_{1z}\overline{\chi}_2\chi_4\overline{\chi}_4, \tag{35'}$$

$$\Phi_3 = \chi_{1x}\chi_{1y}\chi_{1z}\overline{\chi}_{1z}\overline{\chi}_2\chi_4\overline{\chi}_4, \tag{35''}$$

$ArOH_a^+H_b$:

$$\Phi_4 = \chi_{1x}\chi_{1y}\overline{\chi}_{1y}\chi_{1z}\overline{\chi}_3\chi_4\overline{\chi}_4, \tag{36}$$

$$\Phi_5 = \chi_{1x}\overline{\chi}_{1x}\chi_{1y}\chi_{1z}\overline{\chi}_3\chi_4\overline{\chi}_4, \tag{36'}$$

$$\Phi_6 = \chi_{1x}\chi_{1y}\chi_{1z}\overline{\chi}_{1z}\overline{\chi}_3\chi_4\overline{\chi}_4, \tag{36''}$$

$ArO^-H_a^+H_b^+$:

$$\Phi_7 = \chi_{1x}\chi_{1y}\overline{\chi}_{1y}\chi_{1z}\overline{\chi}_{1z}\chi_4\overline{\chi}_4, \tag{37}$$

$$\Phi_8 = \chi_{1x}\overline{\chi}_{1x}\chi_{1y}\chi_{1z}\overline{\chi}_{1z}\chi_4\overline{\chi}_4, \tag{37'}$$

$$\Phi_9 = \chi_{1x}\overline{\chi}_{1x}\chi_{1y}\overline{\chi}_{1y}\chi_{1z}\chi_4\overline{\chi}_4. \tag{37''}$$

Next the Ar^+H_2O configuration and the basis functions which correlate with the asymptotic atomic configurations $Ar^+OH_aH_b$, $Ar^+O^-H_aH_b^+$, and $Ar^+O^-H_a^+H_b$ are considered. Since an arbitrary 3-dimensional geometry has to be described we have

to include all orientations of the 2p AO of O and not only those presented by the H_2O basis functions (3)-(5). This provides $(3 \times 3 =)9$ basis functions of Ar^+H_2O. We have to distinguish also between the states with different atomic spin orientations in H_2O relative to the Ar^+ spin which is assumed to be $S_z = \frac{1}{2}$. As a result, the number of diabatic electronic configurations is doubled so that the number of basis functions becomes $(9 \times 2 =)18$. We shall present below some of the Ar^+H_2O basis functions Φ_k omitting those of them with expressions that can be easily derived. The configurations with positive and negative O atom spin orientation are described by Φ_k with odd and even k, respectively.
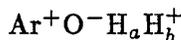
$Ar^+OH_aH_b$

$$\Phi_1 = \chi_{1x}\chi_{1y}\overline{\chi}_{1y}\chi_{1z}\overline{\chi}_2\overline{\chi}_3\chi_4, \tag{38}$$

$$\Phi_2 = \overline{\chi}_{1x}\chi_{1y}\overline{\chi}_{1y}\overline{\chi}_{1z}\chi_2\chi_3\chi_4, \tag{38'}$$

$$\Phi_3 = \chi_{1x}\overline{\chi}_{1x}\chi_{1y}\chi_{1z}\overline{\chi}_2\overline{\chi}_3\chi_4, \tag{38''}$$

$$\Phi_5 = \chi_{1x}\chi_{1y}\chi_{1z}\overline{\chi}_{1z}\overline{\chi}_2\overline{\chi}_3\chi_4, \tag{38'''}$$

$Ar^+O^-H_aH_b^+$

$$\Phi_7 = \chi_{1x}\chi_{1y}\overline{\chi}_{1y}\chi_{1z}\overline{\chi}_{1z}\overline{\chi}_2\chi_4, \tag{39}$$

$$\Phi_8 = \overline{\chi}_{1x}\chi_{1y}\overline{\chi}_{1y}\chi_{1z}\overline{\chi}_{1z}\chi_2\chi_4, \tag{39'}$$

$$\Phi_9 = \chi_{1x}\overline{\chi}_{1x}\chi_{1y}\chi_{1z}\overline{\chi}_{1z}\overline{\chi}_2\chi_4, \tag{39''}$$

$$\Phi_{11} = \chi_{1x}\overline{\chi}_{1x}\chi_{1y}\overline{\chi}_{1y}\chi_{1z}\overline{\chi}_2\chi_4, \tag{39'''}$$

$Ar^+O^-H_a^+H_b$

$$\Phi_{13} = \chi_{1x}\chi_{1y}\overline{\chi}_{1y}\chi_{1z}\overline{\chi}_{1z}\overline{\chi}_3\chi_4, \tag{40}$$

$$\Phi_{18} = \chi_{1x}\overline{\chi}_{1x}\chi_{1y}\overline{\chi}_{1y}\overline{\chi}_{1z}\chi_3\chi_4, \tag{40'}$$

The off-diagonal matrix elements between the states with different oxygen AO orientation coincide with those (see Eqs.(15)-(17) and (26)-(27)) of the $(H_2O)^+$ and H_2O molecules. The coupling between the Ar^+H_2O states with different AO spin orientation (between Φ_1 and Φ_2 of Eqs.(38), for example) is taken into account by the $^1\Sigma$ states of the O^-H fragment. We will treat this coupling in a way similar to the way the H^+H — HH^+ coupling was treated (see Sec.2.1). The O^-H adiabatic potentials

9

are presented as the eigenvalues of Eq.(10). In the O^-H case the diabatic states are distinguished by the atomic spin orientation

$$\phi_1 = \chi_{1\pi}\overline{X}_{1\pi}\chi_{1\pi'}\overline{X}_{1\pi'}\chi_{1\sigma}\overline{X}_2, \tag{41}$$

$$\phi_3 = \chi_{1\pi}\overline{X}_{1\pi}\chi_{1\pi'}\overline{X}_{1\pi'}\overline{X}_{1\sigma}\chi_2. \tag{41'}$$

The coupling between the diabatic electronic configurations of Ar^+H_2O (Eqs.(38)-(40)) and $Ar(H_2O)^+$ (Eqs.(35)-(37)) is taken into account by the $^1\Sigma$ state of the $(ArH)^+$ fragment. The adiabatic potentials of the $(ArH)^+$ fragment are the eigenvalues of the equation

$$\begin{vmatrix} U_{ArH^+} - E & V_{(ArH)^+} \\ V_{(ArH)^+} & U_{Ar^+H} - E \end{vmatrix} = 0 \tag{42}$$

and consequently U_{ArH^+} and U_{Ar^+H} are:

$$U_{ArH^+} = \frac{1}{2}[W_{(ArH)^+}(X\,^1\Sigma) + W_{(ArH)^+}(2\,^1\Sigma) - W_d], \tag{43}$$

$$U_{Ar^+H} = \frac{1}{2}[W_{(ArH)^+}(X\,^1\Sigma) + W_{(ArH)^+}(2\,^1\Sigma) + W_d], \tag{43'}$$

where

$$W_d = \sqrt{[W_{(ArH)^+}(2\,^1\Sigma) - W_{(ArH)^+}(X\,^1\Sigma)]^2 - 4V^2_{(ArH)^+}} \tag{44}$$

3. Diatomic potentials

The required adiabatic potentials to evaluate matrix elements can be taken from empirical studies or *ab initio* calculations. In our treatment, however, most of the excited diatomic potentials are considered as fitting functions with adjustable parameters. While doing that we keep as much as possible their character and generally known features from empirical studies or *ab initio* calculations.

The diatomic potentials of the ionic molecules of the type A^+B or A^-B^+ are presented as a sum of a short range valence potential U_v and a long range electrostatic potential U_{el}

$$U = U_v + U_{el}. \tag{45}$$

In the case of an asymptotic configuration with one charged atom, for example A^+B, the electrostatic interaction is of a polarization origin

$$U_{el} = P(R) = -a_B\,\gamma(R)/R^4, \tag{46}$$

10

where R is the interatomic separation, a_B is the polarization coefficient of the neutral atom B, and γ is a dumping term introduced to prevent the unphysical behaviour of P(R) at small separations R. The suggested form for the functional dependence $\gamma(R)$ is[8]

$$\gamma(R) \;=\; R^4/[R^{12} + (r_{A^+} + r_B)^{12}]^{1/3} \tag{47}$$

with r_{A^+} and r_B being the atomic radii. A suggested form for the attractive $A^+ B^-$ Coulomb potential is

$$U_{el} \;=\; U_c \;=\; -U_0/[R^4 + (r_{A^+} + r_{B^-})^4]^{1/4} \tag{48}$$

where U_0 is equal to 14.4eVÅ. The term $(r_{A^+} + r_{B^-})^4$ in Eq.(48) prevents the unphysical behaviour of U_c at small separations R.

3.1 O-H potentials

The matrix elements (6)-(9) of H_2O and (22)-(24) and (31)-(32) of $(H_2O)^+$ include, in particular, adiabatic and diabatic potentials of the diatomic fragments OH, $(OH)^+$, and $(OH)^-$. Since the diabatic potentials are expressed in terms of the adiabatic ones (see Eqs.(11),(13)) we will discuss the adiabatic potentials only.

The OH potentials are: $X\,^2\Pi$, $3\,^2\Pi$, $C\,^2\Sigma^+$, $1\,^2\Sigma^-$. The OH ground and excited states, i.e. $X^2\Pi$ and $1\,^2\Sigma^-$ respectively have the atomic ground states $O(^3P)$ and $H(^2S)$ as dissociation limit. The OH excited states $3\,^2\Pi$ and $^2\Sigma^+$ have $O^-(^2P)$ and H^+ as dissociation limit. Except for the $1\,^2\Sigma^-$ state which is repulsive the other three terms are bound.[23-25] The ground state $X\,^2\Pi$ potential is described in terms of a modified Morse potential[26] which fits the *ab initio* results of Ref.23. The OH excited state potentials are considered as fitting functions with adjustable parameters. The potentials $3\,^2\Pi$ and $1\,^2\Sigma^-$ which correlate asymptotically with O^-+H^+ include the attractive Coulomb term (48). As it was mentioned above (see Eq.(12)) that the $^2\Pi$ diabatic potentials are coupled with each other and therefore an exchange term V_Π is required which will be considered as a fitting function.

The $(OH)^+$ adiabatic potentials are: $X^3\Sigma^-$ and $A^3\Pi$. Both are bound. The ground state $X\,^3\Sigma^-$ potential which has the $O(^3P) + H^+$ as dissociation limit is presented as a sum of a Morse potential and the polarization term (46) (it fits reasonable well the *ab initio* results of Ref.23). The excited state $A\,^3\Pi$ potential has $O^+(^4S) + H$ as

dissociation limit[27] and is also presented as a sum of a Morse potential (with adjustable parameters) and the polarization term (46).

The $(OH)^-$ potentials are: $X\,^1\Sigma^+$, $2\,^1\Sigma^+$ and $^1\Pi$. All of these states have the $O^-(^2P)+H$ as the dissociation limit. The $(OH)^-$ ground state which is bound[23] is presented as a sum of a Morse potential and a polarization term (46). The dissociation energy of the $X\,^1\Sigma$ state is considered as an adjustable parameter. In contrast to the bound state the excited states are repulsive.

3.2 H-H potentials

The H_2O and $(H_2O)^+$ matrix elements include the excited $^3\Sigma_u$ H_2 potential, the ground $^2\Sigma_g$ and excited $^2\Sigma_u$ potentials of H_2^+, and the $^1\Sigma$ potential of the H^+—H^+ repulsion. The repulsive $^3\Sigma_u$ potential is presented in terms of a modified anti-Morse potential[20] which fits the ab initio results.[28] The $^2\Sigma_g$ and $^2\Sigma_u$ potentials of H_2^+ are assumed to be Morse and anti-Morse potentials, respectively, which fit the results of an accurate calculation.[29]

3.3 Ar-H potentials

The $(ArH_2O)^+$ matrix elements include a van der Waals (vdW) potential $X\,^2\Sigma$ of ArH,[30] three $(ArH)^+$ potentials of the type $X\,^1\Sigma$, $2\,^1\Sigma$, and $^3\Sigma$, and a $1\,^2\Sigma$ Coulomb potential of Ar^+H^+. In the $(ArH)^+$ molecule the ground state $X\,^1\Sigma$ has the $Ar+H^+$ as the dissociation limit whereas the excited states $2\,^1\Sigma$ and $^3\Sigma$ dissociate into Ar^++H. Since we replaced the Ar^+ 3p-AO by an s-AO (see Ch.2) we cannot distinguish between the $(ArH)^+$ and Ar^+H^+ potentials and the known adiabatic potentials of these molecules.[31−33] We assume, however, that the approximated ground state $X\,^1\Sigma$ potential coincides with the real $(ArH)^+$ ground state potential. This potential, presented as a sum of a Morse potential and the Ar^+H polarization term (46), fits the known ab initio potential.[20,31] The excited state potentials of $(ArH)^+$ are presented as a sum of an anti-Morse potential and the H^+Ar polarization term (46). The Ar^+H^+ potential is presented in terms of a repulsive Coulomb potential.

3.4 Ar-O potentials

The matrix elements include the following Ar-O diabatic potentials: the $^3\Sigma^-$ and

$^3\Pi$ of ArO, the $^2\Sigma^-$, $^4\Sigma^-$, $^2\Pi$, and $^4\Pi$ of Ar$^+$O, the $^2\Sigma^+$ and $^2\Pi$ of ArO$^-$, and the $^3\Pi$, $^1\Pi$, $^2\Sigma^-$, and $^4\Sigma^-$ of Ar$^+$O$^-$. Unfortunately, no *ab initio* calculations of Ar-O interactions are known to us. Some indirect information can be obtained from the empirical study of ArO diatomic in the excited $^1\Sigma^+$ state[34] and from semiempirical calculation for the ArOH system.[35] A general idea about the behaviour of the argon-oxygen potentials in different states can be obtained from *ab initio* calculations of diatomics with similar electronic structure. For instance, the ArO$^-$ electronic structure is similar to that of the well studied ArF molecule[36] and the Ar$^+$O$^-$ electronic structure is similar to that of FCl.[37]

Due to lack of Ar–O potentials (and their ions) these had to be constructed . In doing that we took into account the Ar and O radii, as well as some indirect information mentioned before. The ion-atom and ion-ion potentials include the electrostatic terms (46) and (48), respectively. It is important to note that argon-oxygen potentials parameters cannot be treated as adjustable parameters, like it was done in the case of some of the O-H potentials, since there is not available any data to be employed.

4. 3-center term

In order to improve the results (see the following Section) we incorporated into the (H$_2$O)$^+$ matrix elements the so called 3-center term. [26,38] In the (H$_2$O)$^+$ case the suggested 3-center term is

$$W_{3c} \; = \; -g \, exp[-S] \, (1 + b \, sin^2\theta) \tag{49}$$

where

$$S \; = \; \alpha \, [(R_{1,2} - R_0)^2 \, + \, (R_{1,3} - R_0)^2], \tag{49'}$$

θ is the HOH angle, $R_{1,2}$ and $R_{1,3}$ are the O-H distances. The parameters of Eqs.(49) are as follows: $g = 1.2 eV$, $b = 0.22$, $\alpha = 3 \mathring{A}^{-2}$, $R_0 = 1.03 \mathring{A}$.

5. The results of H_2O and $(H_2O)^+$ calculation

The adjustable parameters of the excited diatomic potentials (Ch.3) and the 3-center term (Ch.4) were used to fit, at least approximately, the known empirical and/or *ab initio* parameters of the H_2O molecule and the $(H_2O)^+$ ion.

The results for the ground state $\tilde{X}\,^1A_1$ H_2O molecule calculation are presented in Table 1. These are compared with the H_2O empirical parameters as well as with the parameters obtained from the DIM and the *ab initio* calculations. It is noticed that our calculation provides an H_2O geometry which is very close to the empirical one. In addition our vibrational frequencies are in reasonable agreement with the empirical and the *ab initio* frequencies. On the other hand our calculated dipole moment is about 25% lower than the empirical value so that the Ar^+–H_2O electrostatic interaction is underestimated. Also, our calculated H_2O energy E_e is higher than the empirical value by about 0.66eV. This may look like a significant discrepancy however we are interested in the energy gaps between the different states and not in the absolute values. These energy gaps, as it will be shown below, are of much higher accuracy.

The results of the ground state $\tilde{X}\,^2B_1$ $(H_2O)^+$ calculation are presented in Table 2. The calculated $(H_2O)^+$ energy is higher than the empirical value by 0.56eV but the difference between the $(H_2O)^+$ and H_2O energies is reasonable close to the H_2O ionization potential.

As was mentioned in the Introduction the $(H_2O)^+$ is formed in the excited electronic state $\tilde{A}\,^2A_1$. The various calculated parameters related to the $\tilde{A}\,^2A_1$ $(H_2O)^+$ are presented in Table 3. Like in the *ab initio* calculations[43,45] the equilibrium of the $(H_2O)^+$ geometry in the $\tilde{A}$ state is collinear (in this geometry the $\tilde{A}$ PES is tangent to the ground state of the $\tilde{X}$ PES) but the equilibrium bond length is found to be somewhat larger than the *ab initio* value. The following parameters: the $\tilde{X} \to \tilde{A}$ excitation energy, the excess energy ΔE related to the $\tilde{X} \to \tilde{A}$ transition (for the $\tilde{A}$ equilibrium energy), and the vibrational frequencies ω, all lie in a reasonable proximity of the corresponding parameters of the *ab initio* calculations[43,45] (as well as with these of the empirical model[46]). The exceptional case is the bending frequency which fits the one by Brommer at al.[45] but differ significantly from the one by Smith at al.[43]

The $\tilde{A}$ state $(H_2O)^+$ ion formed in the charge transfer reaction (1) is expected to be found in highly excited vibrational bending states $(0,v_2,0)$.[1] Since the vibrational

bending levels play an important role in the study of the charge transfer reaction we calculated them for the $\tilde{A}$ PES. These calculations were done for the overall rotational state K=0. The calculated vibrational modes are presented in Table 4.

In order to study the stretching–bending coupling effect on the vibrational bending modes calculations were done twice. In the first (column I in Table 4) the stretching motion is restricted to the zero mode $v_1 = v_3 = 0$ so that the stretching–bending coupling effect is of a negligible importance. According to this calculation the energy gaps $\hbar\omega$ between the bending levels are almost constant for low bending levels but increase once $v_2 > 4$. In other treatments of the bending modes[45−46] the energy gaps increase with v_2 from the very beginning.

In the second treatment (column II in Table 4) the stretching modes as well as the stretching–bending couplings were taken into account. While comparing the results of the two calculations (Table 4) it is noticed that the main effect of the coupling is in lowering the bending levels. This effect is stronger the larger is v_2. For instance, the (0,1,0) level is almost the same according the two calculations whereas the (0,9,0) level becomes lower by 0.22eV according the second calculation. Due to the levels shift caused by the stretching–bending coupling the energy gaps between the various bending states remain almost constant along the whole studied interval, i.e. $2 \leq v_2 \leq 12$. Thus according to our treatment the stretching–bending couplings affect significantly the bending levels manifold and it follows that the bending levels obtained within the rigid OH bond approximation are far from being accurate.

6. $(ArH_2O)^+$ potential energy surfaces

A charge transfer reaction can be treated within the electrostatic approximation if the electron transition occurs at intermolecular distances exceeding the strong coupling range. Using the PESs of the present calculation it is possible to estimate this range and consequently to determine the limits of the electrostatic approximation.

Let us consider first the dependence of the $(ArH_2O)^+$ PESs on the HOH valence angle ϑ (Fig.2). These PESs were obtained for Ar^+ ion approaching one of the H atoms along the O–H line (z-axes of Fig.1). The OH distances of the H_2O molecule are fixed and equal to the OH equilibrium distance (0.958Å). The PESs of Fig.2 demonstrate a typical avoided crossing between two electronic states at $\vartheta \approx 108° − 110°$, close to the

15

equilibrium angle of 104.8°. Since the region of the avoided crossing is accessible in the vibrational ground state the bending motion may induce the charge transfer. The avoided crossing gap ΔE increases when the oxygen–argon distance R_{OAr} decreases and becomes comparable to the electrostatic potential at the distance $R_{OAr} \approx 5\text{Å}$.

The adiabatic PESs dependence on the argon position along a straight-line trajectory (see Fig.3) is shown in Fig.4a for a fixed (equilibrium) H_2O geometry. The PESs are presented for three electronic states, namely k=2,4,5. (The ground state k=1 is omitted as it asymptotically correlates with $(H_2O)^+$ in the ground state $\tilde{X}$ and the state k=3 is ignored as it is not coupled with the states of interest due to a different symmetry.) The charge delocalization caused by the electronic coupling is demonstrated in Fig.4b. According to the results of the calculation the effect of the coupling is negligible small at distances $|\rho| > 5\text{Å}$ but becomes relatively strong when $|\rho| \approx 3\text{Å}$ which leads to the deformation of the potential curves (Fig.4a) and to charge delocalization (Fig.4b). Due to this coupling the k=2 potential curve of Fig.4a (which correlates asymptotically with $Ar^+ + H_2O$) decreases as $|\rho|$ decreases and the k=4 potential (which correlates asymptotically with $Ar + (H_2O)^+$) increases. Since the charge delocalization takes place when the states k=2,4 start to diverge the charge is located on both, on Ar and on H_2O . Whereas around $\rho = 0$ the k=5 electronic state becomes the one with the largest Ar charge the opposite is encountered for the k=4 state where the charge is mainly located on H_2O . The regions where the charge distribution is most affected (those are the regions of the avoided crossing) are those in the vicinity of $|\rho| \approx 3.5\text{Å}$ (2 → 4) and $|\rho| \approx 1\text{Å}$ (4 → 5).

For the results presented in Fig.4 (as well as those in Fig.2), the range of the strong–coupled region was found to be roughly equal to 4Å. Comparing this value with the reactive interaction range R_{re} it is possible to conclude whether the electrostatic approximation is valid or not. We suggest to determine R_{re} as the average impact parameter

$$R_{re} = \sqrt{\frac{\sigma}{\pi}} \qquad (50)$$

where σ is the reactive cross section. At near–thermal energies the cross section of the Eq.(1) charge transfer reaction is very large, i.e. 50-60Å^2.[47] The respective reactive interaction range of Eq.(50) is about 4Å, the same as the strong-coupling range. The conclusion can be made that the near-thermal reaction can be treated most probably by the electrostatic approximation. At the suprathermal collision energies of 1–10eV

the reaction cross section is 12-18Å^2.[47] The respective R_{re} values are 2-2.4Å. It follows that in this energy interval the electron hop occurs mainly in the strong–coupling region so that the description of the reaction in the terms of electrostatic interactions is not always sufficient.

7. Charge–transfer reaction study

The charge transfer reaction is expected to be governed by the complex formation at low collision energies and by a direct mechanism at suprathermal energies.[48] In the forthcoming theoretical treatment we consider the suprathermal collision energy region. Also in what follows we will refer to the $(H_2O)^+$ in the first excited electronic $\tilde{A}$ state exclusively.

The H_2O energy in the vibrational ground state (0,0,0) is -8.83eV (Table 1) and the Ar ionization potential is 15.76eV so that the energy of the reagents in reaction (1) is 6.93eV. The energy of the products (the Ar and the $\tilde{A}$ $(H_2O)^+$ in the vibrational ground state) is 4.99eV (Table 4), so that the energy difference is equal to 1.94eV. This excess energy is converted into the internal energy of the $(H_2O)^+$ ion.[1,47] However, as the equilibrium geometries of the reagent H_2O and the product $(H_2O)^+$ differ significantly in their valence angles (104.8° versus 180°) the bending (and not the stretching) modes are the ones expected to be excited. This expectation was confirmed experimentally.[1]

In the energy interval $1 \leq E \leq 10$eV the collision time is of the order of $4 \cdot 10^{-14} - 2 \cdot 10^{-13}$sec. The duration of the H_2O rotation is usually longer and we may assume the fixed rotor approximation. The collision time, however, is much longer than the H_2O bending mode period which is $\sim 2 \cdot 10^{-14}$sec.[45] Consequently the H_2O molecule has the time to cross more then once the avoided crossing region (Fig.2) with some probability to form the $(H_2O)^+$ in the vibrationally excited $(0,v_2,0)$ state. This state can be considered as being near–resonant to the ground state level of the reactants $Ar^+ + H_2O$ system.

At large distances the reactants $Ar^+ + H_2O$ ground state (E=6.93eV) overlaps with the (0,9,0) vibrational bending state of the products $Ar^+ + (H_2O)^+$ (E=6.93eV, see Table 4 column II). In the absence of the stretching–bending coupling (Table 4 column I) the reactants ground state is in near resonance with the products (0,8,0) level, in accordance with the model calculations of Ref.1. In the interaction region of the two

17

molecular species the energies of both, reagents and products, are shifted so that the $(0,0,0)$ Ar^+H_2O vibrational level may overlap with the $Ar(H_2O)^+$ $(0,v_2,0)$ levels whose v_2 is different from the one found in the asymptotic region. In order to study the behaviour of the Ar^+H_2O and $Ar(H_2O)^+$ levels we performed two kinds of calculations. In both we assumed that the argon ion (atom) is approaching (and receding) the water molecule along a straight-line trajectory.

7.1 The simplified treatment

In the simplified treatment it is assumed, like in Ref.1, that the geometry of the water molecule (ion) is not affected by the Ar ion (atom) and that the system energy is equal to the sum of a PES W and a vibrational energy E_v of an isolated molecule

$$E(\rho; b, \gamma, v_2) = W(\rho; b, \gamma) + E_v(v_2) \qquad (51)$$

In Eq.(51) ρ is a coordinate along the Ar trajectory (Fig.3), b is the impact parameter, and γ comprises the intermolecular orientation. The diabatic energy levels along a straight-line trajectory at an impact parameter b=3Å are shown in Fig.5 for three different H_2O orientations. Fig.5 presents energy levels of both, reagents Ar^+H_2O and products $Ar(H_2O)^+$ systems. In the case of the Ar^+H_2O system W is the PES of the frozen (equilibrium) H_2O and E_v is the vibrational energy of the isolated H_2O and in the case of $Ar(H_2O)^+$ system W is the PES of the frozen (equilibrium) $(H_2O)^+$ and E_v is the vibrational energy of isolated $(H_2O)^+$. The $(H_2O)^+$ E_v results follow for the exact calculation (see Table 4 column II).

It is seen in Fig.5 that at large distances the $Ar(H_2O)^+$ levels form a flat manifold for all $(H_2O)^+$ orientations. When the distance becomes relatively small the levels are slightly decreasing due to the attractive ion-induced polarization forces which are isotropic. The behaviour of the reagents Ar^+H_2O level is different due to charge-dipole forces which are much stronger than the polarization forces and can be either attractive or repulsive depending on the H_2O orientation. In the case of Fig.5a (the relevant orientation is shown in Fig.3) the charge–dipole interaction is repulsive and consequently the Ar^+H_2O level is increasing when $|\rho|$ decreases. In the vicinity of $\rho = 0$ the direct repulsion between the Ar^+ and H contributes to a further increase of the Ar^+H_2O energy. As a result the reagents Ar^+H_2O level crosses four $Ar(H_2O)^+$ levels. In case of Fig.5b for the presented orientation the charge–dipole interaction is attractive but in the vicinity of $\rho = 0$ this electrostatic interaction is compensated

by the direct interatomic repulsion. There are no level crossings in this case. Fig.5c presents the case of a different interactions for incoming and outgoing trajectories. In particular, the charge–dipole interaction is attractive for $\rho < 0$ and repulsive for $\rho > 0$. In the vicinity of $\rho = 0$, because of the proximity of the argon atom to one of the hydrogen atoms, a strong repulsion is demonstrated. The Ar^+H_2O ground vibrational level of Fig.5c crosses a few times the $Ar(H_2O)^+$ excited levels. According to Fig.5 the products $(H_2O)^+$ which is formed along the b=3Å trajectory is formed in different vibrational bending $(0,v_2,0)$ states, namely $v_2 = 8, 9, 10, 11$. We do not consider here the trajectories with the impact parameters $b < 3$Å as the straight-line assumption is most probably not valid anymore.

7.2 Full scale calculation

In contrast to the simplified calculation, in the full scale calculation the H_2O and $(H_2O)^+$ vibrational modes are calculated not for isolated species but in the field of the argon ion (or atom). In Fig.7a are presented the vibrational eigenstates of the Ar^+H_2O and the $Ar(H_2O)^+$ systems as a function of ρ (see Fig.6) and fixed value of b (=3Å), calculated employing average PESs obtained following a rotation around the x-axis (see Fig.6). The two PESs used in the calculation were constructed for the two relevant adiabatic surfaces (obtained by the diagonalization of the DIIS matrix) which then were chosen, for the sake of this calculation, to be diabatic. These two PESs become, once $\rho \rightarrow \infty$, the $Ar^+ + H_2O$ and $Ar + (H_2O)^+$ surfaces. It was found that this procedure holds as long as $\rho \geq 2$Å. The effect of the argon–water interaction on the charge distribution and HOH equilibrium configuration is shown in Fig.7b for the electronic state correlated asymptotically with Ar^+H_2O. While the Ar^+ approaches H_2O the charge concentrates on the HOH fragment so that at relatively small distances ($\rho < 4$Å) the electronic configuration of the system is rather described as $Ar(H_2O)^+$ instead of Ar^+H_2O. The increase of the HOH charge is also accompanied by the increase of the HOH valence angle.

A different situation is encountered in case of the asymptotic $Ar(H_2O)^+$ system. Here the Ar atom remains uncharged up to small values of ρ. Only in the vicinity of $\rho = 0$ the Ar atom acquires small quantities of charge (about 20%). The approaching Ar atom does not affect on the $(H_2O)^+$ equilibrium geometry which remains collinear throughout its approach.

19

The effect of coupling on the $(ArH_2O)^+$ energy levels is shown in Fig.7a. At large distances ($\rho > 5$Å) where the electrostatic forces are dominant the $Ar(H_2O)^+$ levels $(0,v_2,0)$ form a flat manifold, like in the simplified treatment (see Fig.5). The same situation is encountered in the case of Ar^+H_2O $(0,0,0)$ system (this is in contrast to what was observed in the simplified model – see Fig.5). At small ρ values, in the strong-interaction region, all levels decrease. It is important to emphasize that the $Ar(H_2O)^+$ $(0,9,0)$ level is in near resonance with the Ar^+H_2O ground state. In this sense our more extensive treatment differs significantly from the simplified calculation.

Similar results were obtained for other orientations of the HOH rotation axis and therefore they will be not presented here.

8. Conclusions

1. The semiempirical diatomics-in-ionic-systems (DIIS) method proves to be an effective tool for treating the PESs of the $(ArH_2O)^+$ system. Within the DIIS method, like in the DIM, the Hamiltonian matrix elements are expressed in terms of diatomic potentials but in the DIIS along with adiabatic diatomic potentials one employs also the diabatic potentials which describe electronic configurations with localized charges.

2. According to this treatment the product $(H_2O)^+$ ion (see Eq.(1)) formed in the $\tilde{A}\,^2A_1$ state is highly vibrationally (bending) excited. Also it was found that the calculated vibrational bending manifold is strongly affected by the stretching–bending coupling.

3. It is shown that the electrostatic approximation may be applied to the near-thermal reactions only. At suprathermal collision energies this approximation is not valid anymore and the electron hop occurs mainly in the strong coupling region. Also it is established that the electron transfer is induced by the H_2O bending motion and it takes place at the region of Ar^+H_2O—$Ar(H_2O)^+$ avoided crossing.

4. The Ar^+H_2O and the $Ar(H_2O)^+$ vibronic bending modes were calculated by two different ways, a simplified version and a full scale one. In the simplified version the charge is assumed to be located either on the Ar or the H_2O and the effect of Ar^+ (or Ar) on H_2O (or $(H_2O)^+$) is ignored. Consequently it was found that the $(0,0,0)$ state is in near resonance with the $(0,9,0)$ state in the asymptotic region only but then

20

crosses the $Ar+(H_2O)^+$ manifold as the distance decreases. The two assumptions were not included in the full scale versions and as a result we found that (0,0,0) state of $Ar^+ + H_2O$ is in near resonance with the (0,9,0) bending state of the $Ar+(H_2O)^+$ along the whole interaction region.

Acknowledgments

References

1. R.A.Dressler, J.A.Gardner, R.H.Salter, and E.Murad, *J.Chem.Phys.* 96, 1062 (1992)

2. S.Chapman and R.K.Preston, *J.Chem.Phys.* 60, 650 (1974)

3. M.Baer and J.A.Beswick, *Phys.Rev.* A 19, 1559 (1979)

4. S.Chapman, *J.Chem.Phys.* 82, 4033 (1985)

5. M.Baer and H.Nakamura, *J.Chem.Phys.* 87, 4651 (1987)

6. S.Chapman, in State-Selected and State-to-State Ion-Molecule Reaction Dynamics, Part 2, Ed. M.Baer and Ch.-Y.Ng, John Wiley & Sons, 1992, p.423

7. P.J.Kuntz and A.C.Roach, *J.Chem.Soc.Far.Trans.* II 68, 259 (1972)

8. I.Last and T.F.George *J.Chem.Phys.* 93, 8925 (1990)

9. E.A.Gislason, G.Parlant, and M.Sizun, in State-Selected and State-to-State Ion-Molecule Reaction Dynamics, Part 2, Ed. M.Baer and Ch.-Y.Ng, John Wiley & Sons, 1992, p.321

10. P.Archirel and B.Levy, *Chem.Phys.* 106, 51 (1986)

11. B.R.Diaz and P.Wahnon, *Chem.Phys.Lett.* 212, 218 (1993)

12. C.Y.Dykstra, *J.Mol.Struct.* 103, 131 (1983)

13. E.D.Simandiras, J.F.Gaw and N.C.Handy, *Chem.Phys.Lett.* 141, 166 (1987)

14. F.O.Ellison *J.Am.Chem.Soc.* 85, 3540 (1963)

15. P.J.Kuntz, in Atom-Molecule Collision Theory, Ed. R.B.Bernstein, Plenum Press, N.Y.-London, 1979, p.79

16. J.C.Tully, *J.Chem.Phys.* 60, 3042 (1974)

17. M.B.Faist and J.T.Muckerman, *J.Chem.Phys.* 71, 225 (1979)

18. I.Last, *Chem.Phys.* <u>55</u>, 237 (1981)

19. I.Last and T.F George, in Cluster Ions, Ed. Ch.-Y.Ng, T.Baer and I.Powis, John Wiley & Sons, 1993, Ch.6, p.319

20. I.Last and T.F.George *J.Chem.Phys.* <u>87</u>, 1183 (1987)

21. J.C.Tully, *J.Chem.Phys.* <u>58</u>, 1396 (1973)

22. R.Polak, I.Paidarove, and P.J.Kuntz, *J.Chem.Phys.* <u>87</u>, 2863 (1987)

23. H.-J.Werner, P.Rosmus, and E.-A.Reinsch, *J.Chem.Phys.* <u>79</u>, 905 (1983)

24. E.F.van Dishoeck and A.Dalgarno, *J.Chem.Phys.* <u>79</u>, 873 (1983)

25. S.R.Langhoff, Ch.W.Bauschlicher,Jr., and P.R.Taylor, *J.Chem.Phys.* <u>91</u>, 5953 (1989)

26. I.Last and M.Baer, *J.Chem.Phys.* <u>75</u>, 288 (1981)

27. R.P.Saxon and B.Liu, *J.Chem.Phys.* <u>85</u>, 2099 (1986)

28. W.Kołos and C.C.J.Roothaan, *Rev.Mod.Phys.* <u>32</u>, 219 (1960)

29. D.R.Bates, K.Ledsham, and A.L.Steward, *Philos.Trans.Soc.London* <u>246</u>, 215 (1953)

30. H.Partridge, D.W.Schwenke, and Ch.W.Bauschlicher,Jr., *J.Chem.Phys.* <u>99</u>, 9776 (1993)

31. P.Rosmus, *Theor.Chim.Acta* <u>51</u>, 359 (1972)

32. V.Sidis, *J.Phys.* B <u>5</u>, 1517 (1972)

33. J.Lundell, J.Nieminen, and H.Kunttu, *Chem.Phys.Lett.* <u>208</u>, 247 (1993)

34. J.F.Liebman, and L.C.Allen, *Chem.Comm.* N 23, 1355 (1969)

35. Y.Guan and J.T.Muckerman, *J.Phys.Chem.* <u>95</u>, 8293 (1991)

36. Th.H.Dunning,Jr., and P.J.Hay, *J.Chem.Phys.* <u>69</u>, 134 (1978)

37. K.A.Peterson and R.C.Woods, *J.Chem.Phys.* <u>92</u>, 7412 (1990)

38. I.Last and M.Baer, *J.Chem.Phys.* <u>80</u>,3246 (1984)

39. E.A.V.Ebsworth, J.A.Connor. and J.J.Turner, in Comprehensive Inorganic Chemistry, Ed. A.F.Trotman–Dickenson, v.2, p.685, Pergamon Press, Oxford, 1973

40. Th.H.Dunning,Jr., S.P.Walch, and A.F.Wagner, in Potential Energy Surfaces and Dynamics Calculations, Ed. D.G.Truhlar, Plenum Press, New York, 1981, p.329

41. Handbook of Chemistry and Physics, 53rd edition, 1972–1973 Ed. R.C.Weast, The Chemical Rubber Co., Ohio, 1972

42. B.Rosen, Spectroscopic Data Relative to Diatomic Molecules, Pergamon, New York, 1970

43. J.A.Smith, P.Jørgensen, and Y.Öhrn, *J.Chem.Phys.* <u>62</u>, 1285 (1975)

44. B.Weis, S.Carter, P.Rosmus, H.-J.Werner, and P.J.Knowles, *J.Chem.Phys.* <u>91</u>, 2818 (1989)

45. M.Brommer, B.Weis, B.Follmeg, P.Rosmus, S.Carter, N.C.Handy, H.-J.Werner, and P.J.Knowles, *J.Chem.Phys.* <u>98</u>, 5222 (1993)

46. Ch.Jungen, K.-E.J.Hallin and A.J.Merer, *Molec.Phys.* <u>40</u>,25 (1980)

47. R.A.Dressler, R.H.Salter, and E.Murad, *J.Chem.Phys.* <u>99</u>, 1159 (1993)

48. J.A.Gardner, R.A.Dressler, R.H.Salter, and E.Murad, *J.Chem.Phys.* <u>93</u>, 7780 (1990)

Table 1. H_2O properties

	present calc.	Empirical	ab initio[e]	ab initio[b]	DIM[f]	DIM[g]
OH bond length (Å)	0.958	0.957[a]	0.943	0.982	0.999	0.979
HOH angle (deg.)	104.8	104.5[a]	106.7	102.3	10.9	100.3
Dipole moment (D)	1.36	1.87[a]		2.21		
Energy E_e (eV)	-9.412	-10.069[b]		-8.812	-9.868	-9.37
Energy E_0 (eV)	-8.831	-9.605[c]				
(010)	1832	1648[a] 1598[d]	1751			
Vibr. ω (cm^{-1})(001)	3518	3832[a] 3656[d]	4164			
(100)	3898	3943[a]	4261			

[a] Ref. 39   [b] Ref. 40   [c] Ref. 41   [d] Ref. 42   [e] Ref. 43   [f] Ref. 22   [g] Ref. 21

Table 2. $(H_2O)^+$ ground state properties

		Present calc.	Empir.	ab initio[a]
OH bond length	(Å)	1.028	1.001[a]	1.000
HOH angle	(deg.)	112.2	108.9[a]	109.1
Energy E_e	(eV)	3.011		
H_2O ioniz. pot. I	(eV)	12.406	12.62[b]	
Energy E_0	(eV)	3.575	3.015[c]	
	(010)	1711	1388[a]	1477
Vibr. ω (cm^{-1})	(001)	3543	3220[a]	3381
	(100)	3648	3454[a]	3438

[a] Ref. 44   [b] Ref. 39   [c] Calculated as $E_0 + I$ of H_2O (for E_0 see Table 1).

Table 3. $(H_2O)^+$ excited state A $^2A_1$ properties

Geometry			present calc.	ab initio[a]	ab initio[b]	Empir. model[c]
Equilibrium	OH bond length	(Å)	1.008	0.978	0.989	
$(H_2O)^+$ A	Energy E_e	(eV)	4.370			
		(010)	1880	799	1501	1679
	Vibr. ω (cm^{-1})	(001)	3640	3648		
		(100)	4156	3825		
Equilibrium	Energy E	(eV)	5.520			
	$\Delta E = E - E_e$	(eV)	1.150		1.61	1.076
$(H_2O)^+$X	X --> A excit. en.	(eV)	2.510		2.59	2.214
Equil . H_2O	Energy E	(eV)	6.712			

[a]Ref. 43   [b]Ref. 45   [c]Ref. 46

Table 4. Vibronic bending levels $(0,v_2,0)$ of $(H_2O)^+$ in the A $^2A_1$ state (in eV).

v_1 v_2 v_3	I[a] energy levels	$h\omega$	II[b] energy levels	$h\omega$	$h\omega$[c]	$h\omega$[d]
0 0 0	4.995		4.993			
0 1 0	5.235	0.240	5.226	0.233	0.208	0.186
0 2 0	5.474	0.239	5.451	0.225	0.224	0.207
0 3 0	5.712	0.238	5.672	0.221	0.235	0.225
0 4 0	5.952	0.240	5.890	0.218	0.243	0.234
0 5 0	6.194	0.242	6.107	0.217	0.249	0.243
0 6 0	6.441	0.247	6.326	0.219	0.254	0.249
0 7 0	6.691	0.250	6.545	0.219	0.258	0.255
0 8 0	6.947	0.256	6.765	0.220	0.261	0.258
0 9 0	7.205	0.258	6.984	0.219		0.261
0 10 0	7.461	0.256	7.200	0.216		0.264
0 11 0	7.717	0.256	7.420	0.220		0.266
0 12 0	7.988	0.266	7.641	0.221		

[a] Calculation without stretching - bending coupling.
[b] Calculation including the stretching - bending coupling (see text).
[c] Empirical model[46]
[d] Ab initio calculation[45]

Figure captions

Fig.1 The HOH geometry.

Fig.2 The $(ArH_2O)^+$ adiabatic PESs dependence on the HOH valence angle for different argon positions along the z-coordinate (Fig.1).

(a) $z = \infty$ (solid lines) and z=4Å (dashed lines).

(b)   z=6Å (solid lines) and z=5Å (dashed lines).

Fig.3 The $(ArH_2O)^+$ geometry.

Fig.4 (a)   The $(ArH_2O)^+$ adiabatic states as a function of the argon position ρ (see Fig.3) for a fixed HOH geometry of the isolated H_2O and frozen HOH orientation.

(b)   The Ar charge along ρ (for the same conditions described in (a)).

The numbers k=2,4,5 denote the Ar^+H_2O electronic states (see text)

Fig.5 The Ar^++H_2O and $Ar+(H_2O)^+$ diabatic energy levels for fixed HOH geometry and orientation. Dashed line represents the Ar^++H_2O system with the H_2O in the electronic — vibrational ground state (for the situation given in Fig.3a). Solid lines are for the various excited vibrational bending $(0v_20)$ states of the $\tilde{A}\,^2A_1$ $(H_2O)^+$ ion belonging to the $Ar+(H_2O)^+$ system (for the situation described in Fig.3b). The results are for impact parameter b=3Å and for the following geometries:

(a)   The H_2O atoms coordinate are: O(0.065,0,0), H(-0.520,0,±0.759) and the $(H_2O)^+$ atoms coordinates are: O(0,0,0), H(0,0,±1.008).

(b)   The H_2O atoms coordinate are: O(-0.065,0,0), H(0.520,±0.759,0) and the $(H_2O)^+$ atoms coordinates are: O(0,0,0), H(0,±1.008,0).

(c)   The H_2O atoms coordinate are: O(0,0,-0.065), H(±0.759,0,0.520) and the $(H_2O)^+$ atoms coordinates are: O(0,0,0), H(±1.008,0,0).

Fig.6 The Ar^+H_2O geometry for the full scale calculation

Fig.7 (a) Vibrational bending energy levels as a function of ρ for the situation given in Fig.6. Dashed line is for the electronic state correlated asymptotically with $Ar^+ + H_2O$ and solid lines are for the electronic state correlated asymptotically with $Ar + (H_2O)^+$. The results are for impact parameter b=3Å. (More details are given in the text).

(b) The valence HOH angle and Ar atom charge as a function of ρ for the situation given in Fig.6.

— · — ·   HOH valence angle (left axis)

– – – –   Ar charge (right axis)
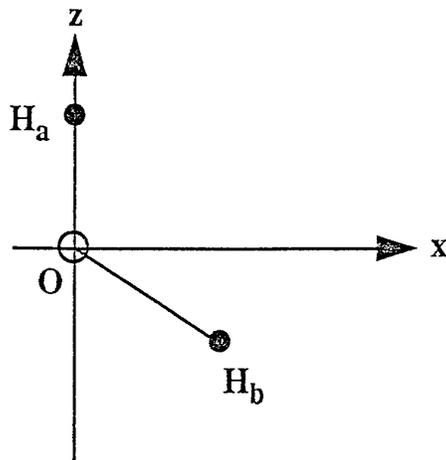
Fig.1
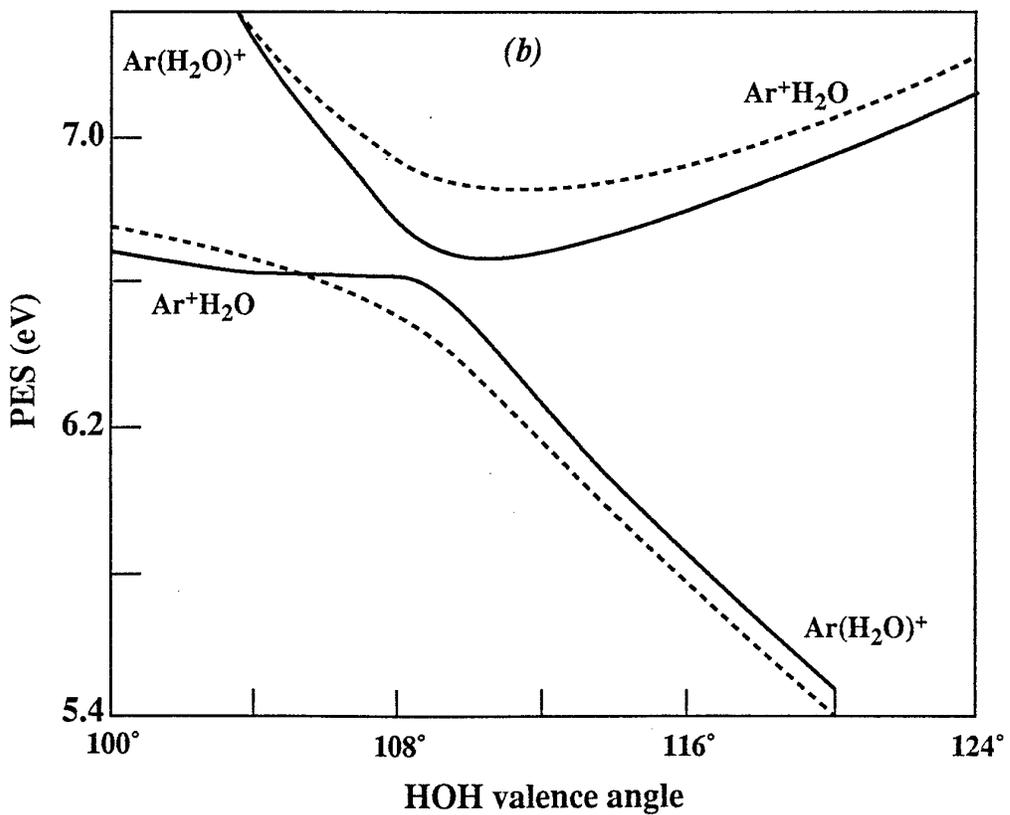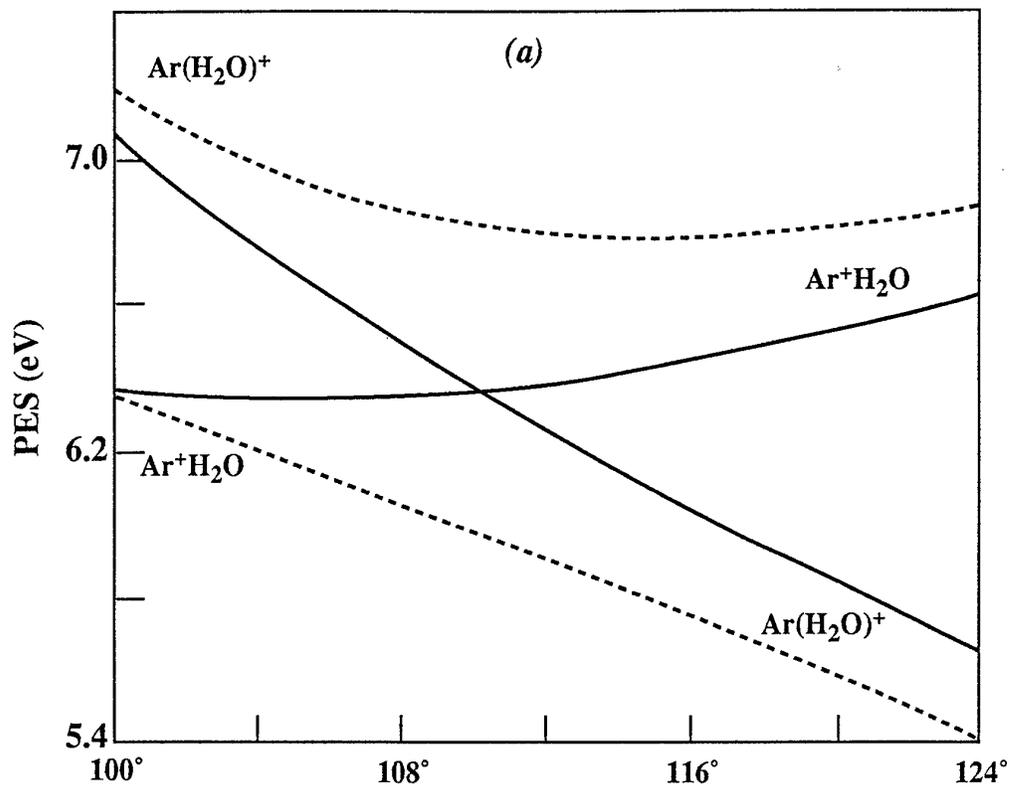
Fig. 2
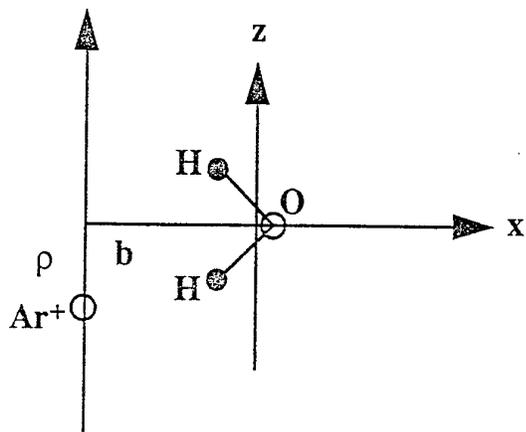
a) $Ar^+ + H_2O$

b) $Ar + (H_2O)^+$

Fig.3

Fig. 4a

(a)

k=5

k=4

k=2

E (eV)

ρ (Å)

Fig. 4b

Fig. 5a

Fig. 5F

E (eV)

ρ (Å)

$v_2=11$

$v_2=10$

$v_2=9$

$v_2=8$

Fig. 5e

Fig.6

a

v₂=10

v₂=9

v₂=8

E (eV)

7.2

6.8

6.4

b

HOH valnce angle

Ar charge

110°

106°

102°

1.0

0.5

0

6   4   2

ρ (Å)

837-e.-IX

fig. 7